Chapter 8
The Structure of Catalysts Studied Using Environmental Transmission Electron Microscopy

Thomas W. Hansen and Jakob B. Wagner

8.1 Introduction

In the chemical industry, approximately 85–90 % of all chemicals are made via catalytic processes (Chorkendorff and Niemantsverdriet 2003). Catalysts are used in processes ranging from synthesis of fine chemicals over fuel refinement to abatement of pollution. Heterogeneous catalysts often comprise metal nanoparticles supported on a substrate providing a high dispersion and stabilization of the particles. The nanoparticle surfaces hold the active sites responsible for the conversion of reactants to products. The atomic arrangement at the specific surfaces has large influence on the reaction rate, making it of high importance to be able to study this arrangement on a local scale. Something, which has become a reality with the advent of aberration corrected transmission electron microscopy (TEM) (Hansen and Wagner 2012; Yoshida et al. 2012). Whereas this information could be obtained from more conventional high vacuum microscopy (Honkala et al. 2005; Carlsson et al. 2006; Janssens et al. 2006), the atomic arrangement, and distribution of specific surfaces are most likely different when the catalyst is in a reactive environment.

During reaction, catalysts are often exposed to harsh environments with high temperatures and corrosive gases inside the reactor resulting in a change of the structure of both active nanoparticles and substrate. Effectively this means that the surface of the nanoparticles can oxidize, be poisoned by adsorbing species, or the particles could sinter resulting in larger particles. All these phenomena result in the loss of active surface area. In order to unravel the dynamic entities as a function of the reaction coordinate, structural and spectroscopic studies under a reactive environment are needed (Grunwaldt et al. 2000).

T.W. Hansen (✉) • J.B. Wagner
Center for Electron Nanoscopy, Technical University of Denmark,
Kgs. Lyngby 2800, Denmark
e-mail: twh@cen.dtu.dk

T.W. Hansen, J.B. Wagner (eds.), *Controlled Atmosphere Transmission Electron Microscopy*, DOI 10.1007/978-3-319-22988-1_8

In situ electron microscopy in general and environmental transmission electron microscopy (ETEM) in particular can provide detailed information on a local scale such as particle size distributions, shape of catalytically active nanoparticles, atomic structure and composition of surfaces, etc.—all giving insight in the gas–solid interactions taking place during catalytic activity (Hansen and Wagner 2014). Such knowledge combined with a quantum chemical treatment of the problem using density functional theory and microkinetical models enables prediction of the conversion of reactants to products and hence derivation of an overall reaction rate (Honkala et al. 2005; Brodersen et al. 2011). However, addressing site-specific turnover numbers (Boudart 1995) remains a daunting challenge.

Although atomic resolution of the catalyst in action is of great importance, the overall performance of a catalytic system is dependent on features at different length scales (Grunwaldt et al. 2013). Electron microscopy has the necessary resolution and flexibility to characterize samples at magnifications spanning five orders of magnitude and has had a large impact in heterogeneous catalysis science (Datye 2003; Hansen et al. 2006; Zhang et al. 2013a; Gai et al. 2007).

Even though electron microscopy in general and ETEM in particular are powerful techniques for the catalyst society, they rely considerably on complementary techniques in order to ensure that local effects probed by TEM are representative for the sample as a whole. As an example, the combination of ETEM and in situ EXAFS has been used for studying the morphology of Cu nanoparticles (Grunwaldt et al. 2000; Hansen et al. 2002a). However, the studies are performed in separate experimental setups. Bringing more characterization techniques together in one instrument might, despite the increased complexity, be a beneficial addendum to the ETEM community. As an example, several groups bring light into the microscope via special TEM sample holders facilitating light input by fiber optics or add the light source directly to the microscope column (Cavalca et al. 2012; Miller and Crozier 2013). Light can be guided out of the microscope in the same way. Cathodoluminescence is already possible with dedicated equipment in the microscope, but to the authors knowledge it has not been reported used in combination with a gaseous environment. Having the light-in and the light-out capabilities, it is straightforward to imagine the combination of electron spectroscopy and optical spectroscopy such as Raman spectroscopy and Plasmon resonance spectroscopy in environmental TEM by optimizing the collection solid angle of the optical response signal.

Recently, more sensitive cameras have been developed for TEM allowing for shorter acquisition times and thereby better temporal resolution of the dynamic processes. These include CMOS-based technology and direct electron detection. Both types have improved sensitivity and read out speed compared to traditional CCD-based cameras. See earlier chapters for more information on electron detection. On the sample holder side, MEMS technology is now extensively used. MEMS technology allows for closed cell sample holders compatible with pressures exceeding atmospheric pressure. Using an MEMS-based close cell holder, Vendelbo et al. were able to correlate shape changes of a platinum nanoparticle with changes in the gas composition at 100,000 Pa total pressure (Vendelbo et al. 2014).

Furthermore, miniaturized heaters can be fabricated, where the heated area is only a few hundred micron resulting in a considerable reduction in drift compared to traditional furnace type holders. More information on MEMS technology and its application to sample holders can be found in a later chapter. Aberration correction has also made its way to ETEM experimentation thus bringing the resolution of the microscopes down to below 1 μm.

Recent development in 4D ultrafast electron microscopy (4D UEM) gives the possibility for imaging processes in the femtosecond regime (Flannigan and Zewail 2012). The basic idea behind these highly specialized TEMs is the synchronization of an electron pulse used for imaging and a stimulus of the sample (e.g., heating). This way, high temporal resolution of irreversible reactions can be obtained. In order to have enough electrons in the electron pulse, to image the sample the density of electrons is so high that Coulomb repulsion is limiting the coherence of the electron beam. That results in a somewhat lower spatial resolution than can be obtained in more traditional TEMs. However, 4D UEM shows great potential for imaging at the time scale of chemical reactions.

8.2 Applications Within Catalysis

For supported catalysts, a parameter of interest is typically the particle size distribution. Unlike many other techniques such as X-ray diffraction (XRD), X-ray photoelectron spectroscopy (XPS), and X-ray absorption spectroscopy (XAS) TEM can provide not only the mean particle size but also the size distribution. Admittedly, such a distribution will be obtained from only a limited subset of the particles where XRD, for instance, can provide an estimate of the average size from a macroscopic amount of the sample. However, TEM can provide information far beyond the particle size distribution. ETEM provides an invaluable tool for supporting the current trend in catalysis of engineering particles with a specific functionality.

As catalytic materials are exposed to various gas species at elevated temperatures, accommodate the change in surface energy caused by adsorbed species by redistributing the area of difference facets. Furthermore, after prolonged exposure to a reactive environment, catalyst nanoparticles tend to deactivate by sintering or poisoning of specific surfaces and their surfaces could restructure. The restructured and often dynamic surface forms the basis for the "active" sites during a catalytic reaction. Although morphology changes of the catalysts are observed under gaseous atmosphere in the ETEM linking it directly to the activity of the catalyst is difficult as quantitative measurements of conversion and selectivity is far from an easy task in the ETEM setup. In the pursuit of measuring reaction products, the group at Arizona State University has made significant progress by measuring the electron energy-loss signal of the gas phase. In this way, they have successfully measured the conversion of carbon monoxide to carbon dioxide (Chenna and Crozier 2012). These efforts are further described in an earlier chapter.

Whereas products of catalytic reactions are challenging to measure in the ETEM, the conditions to which the samples are exposed mimic those found in the catalytic converter, albeit typically at much lower pressure. Still, most of the pressure gap between UHV experimentation and industrial catalysis has been bridged. Experimental observations from a single technique should never stand alone. Interpretations should be done on conjunction with other techniques capable of extending the bridge to fully cover the gap.

Contrary to many other experimental techniques, electron microscopy provides detailed information about specific sites on a local scale. This means that for example the refaceting of an individual nanoparticle as its surroundings vary or the trajectory of individual mobile nanoparticles can be followed. This is not possible with any other technique. The following sections are meant to illustrate the capabilities of the electron microscope within catalysis taking advantage of the recent developments mentioned above.

8.3 On the Active State of Supported Metal Catalysts

8.3.1 Cu/ZnO: Methanol Synthesis

As the environment around metal nanoparticles changes, the fraction of different gases adsorbed on the surfaces changes. This can result in a change of the specific surface energy allowing for a restructuring of the particle. Using the first ETEM equipped with a field emission electron source, Hansen et al. demonstrated this effect on a Cu/ZnO methanol synthesis catalyst (Hansen et al. 2002a).

As summarized in Fig. 8.1, the catalyst was exposed to various environments found in the methanol synthesis reactor: H_2, H_2/H_2O and H_2, CO, all at 220 °C. In pure hydrogen, the copper particles appeared faceted exposing the low-index facets (100), (110), and (111). As the surroundings became more oxidizing by adding H_2O, the particles adopted a more spherical shape due to relative change in the facet-specific surface energies by adsorption of OH species. Under these conditions, the particles remained metallic as determined by HRTEM analysis. When switching the environment to a more reducing environment by adding CO to the hydrogen, the particles again exposed facets but the distribution of the different facets changed and the particle wetted the ZnO surface. Two explanations, which might both contribute to the observed effect, were suggested. First, the surface energy of the copper particles changes as CO adsorbs on the particle surface. Secondly, the surface of the zinc oxide support is slightly reduced offering a different interface energy to the copper particle. In contradiction to the morphology changes observed as an effect of the H_2O treatment, the wetting of the Cu particles was observed to be irreversible when CO was removed after the CO/H_2 treatment indicating that the major effect is caused by surface reduction of the ZnO. The chemical state of the Cu nanoparticles under the different environments was further

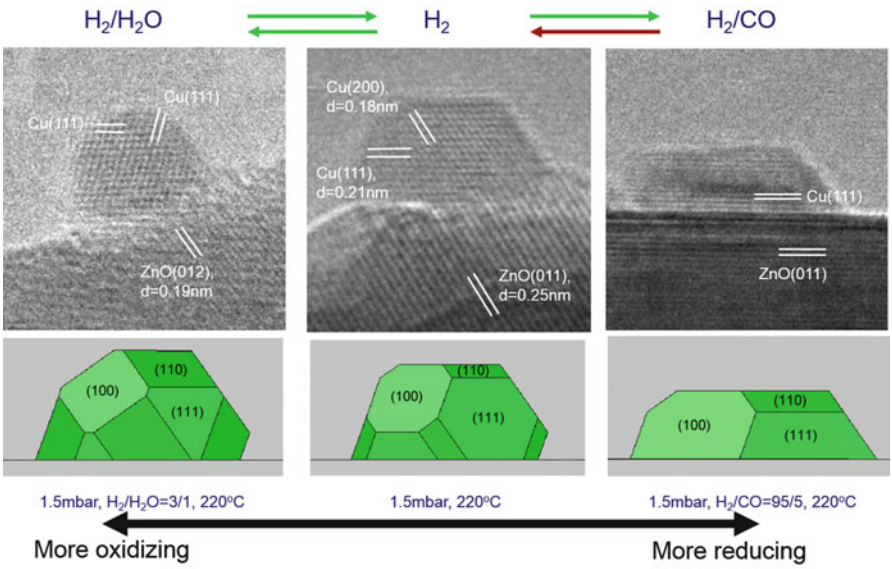

Fig. 8.1 TEM images showing the reversible shape change of a Cu nanoparticle. The same Cu nanoparticle is imaged at 220 °C under (**a**) H_2 at 150 Pa, (**b**) H_2:H_2O (3:1) at a total pressure of 150 Pa, and (**c**) H_2 at 150 Pa. Reproduced from (Hansen et al. 2002a). Copyright 2002 American Association for the Advancement of Science

studied by electron energy-loss spectroscopy (EELS). In all cases described above, Cu was found to be in the metallic state (Wagner et al. 2003). The findings from the ETEM studies were consistent with the results from Grunwaldt et al. who studied a similar catalyst system. Using EXAFS, it was determined that the Cu–Cu coordination number change reversibly during changes in the reaction conditions indicating a morphology change of the Cu nanoparticles (Grunwaldt et al. 2000). The study also confirmed that alloys of Zn and Cu do not form under methanol synthesis conditions. The metallic state of copper under reaction conditions was also confirmed in an infrared spectroscopy (FTIR) study by Topsøe and Topsøe (Topsoe and Topsoe 1999). The morphology change of the Cu particles has been used as input for microkinematical models in order to relate the distribution of facets to the activity (Askgaard et al. 1995; Wagner et al. 2002; Topsøe and Topsøe 1999).

In a more recent study by Cabié et al.(2010), a similar phenomenon was observed for platinum nanoparticles. The platinum nanoparticles were mainly truncated by (001) facets in O_2 and mainly by (111) facets in H_2. Refaceting was again observed when the same set of nanoparticles was re-exposed to oxygen. The same group studied the refaceting further including other catalyst systems including Au and Ag nanoparticles as well (Giorgio et al. 2008; Molina et al. 2011).

8.3.2 Au/Oxides: CO Oxidation

Typically, the outermost layers of a nanoparticle will restructure depending on the composition of the surrounding gas atmosphere. Observing the atomic configuration under a reactive environment is necessary in order to unravel the nature of the active site for a given reaction.

Despite gold being chemically inert in the bulk (Hammer and Nørskov 1995), gold nanoparticles below about 10 nm are highly active for the oxidation of carbon monoxide to carbon dioxide even at temperatures below room temperature (Haruta et al. 1989, 1993). Gold nanoparticles have been studied extensively using electron microscopy, focusing specifically on nanoparticle sizes, surface structure, support interface, and growth (Akita et al. 2013). For gold, nanoparticle growth is particularly important as all activity is lost when the nanoparticles exceed a certain size (Akita et al. 2001).

Using an aberration corrected ETEM, Yoshida et al. investigated gold nanoparticles supported on cerium dioxide (Yoshida et al. 2012). The catalyst was first observed in vacuum, where the surface did not restructure as viewed in the <110> zone axis—see Fig. 8.2. As the sample was exposed to a mixture of 1 % CO in air, the outermost gold layer expanded from 0.20 nm (as also observed in

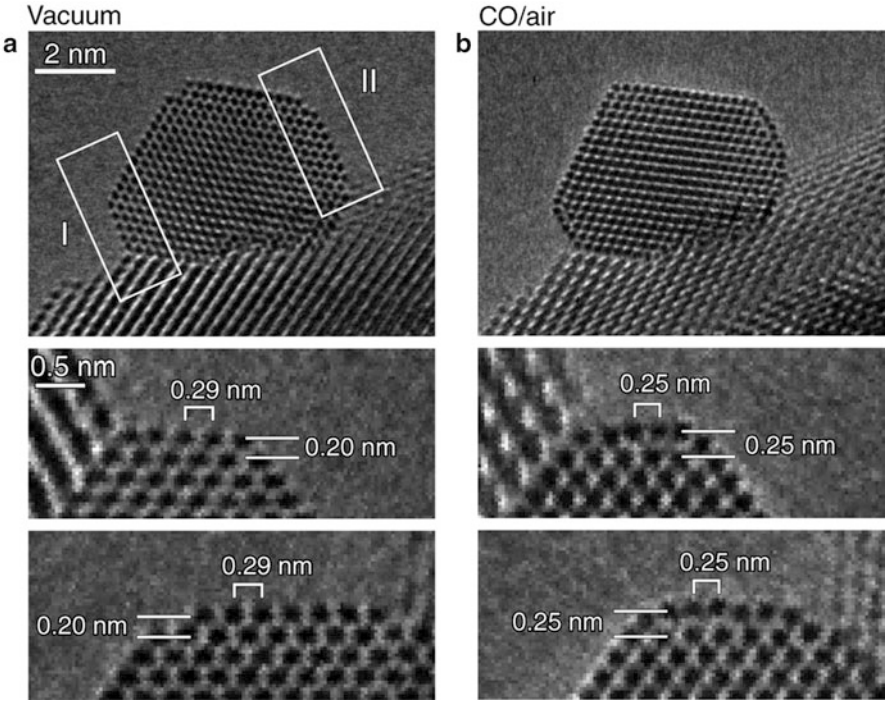

Fig. 8.2 Au {100} reconstructed surface under catalytic conditions. The CeO_2-supported gold nanoparticle in (**a**) vacuum and (**b**) a reaction environment (1 vol.% CO in air gas mixture at 45 Pa at room temperature). Reproduced from (Yoshida et al. 2012). Copyright 2012 American Association for the Advancement of Science

bulk Au) to 0.25 nm. The combination of the ETEM observations with ab initio calculations using the VASP package (Kresse and Hafner 1993) show that the restructured gold nanoparticle surface accommodates a higher surface coverage of CO molecules compared to the bulk terminated structure due to an unusual bonding arrangement with the second gold layer. Similarly, Uchiyama et al. studied the shape of gold nanoparticles supported on cerium oxide in different atmospheres. Their main observations were that when exposed to CO/air mixtures, the gold nanoparticles were truncated by low energy {111} and {100} facets (Uchiyama et al. 2011).

8.3.3 Ru/BN: Ammonia Synthesis

Supported ruthenium nanoparticles have been found to be a highly active catalyst for ammonia synthesis (Jacobsen 2001). Studies of Ru nanoparticles supported on carbon, boron nitride, magnesium aluminum spinel, and alumina have shown these catalysts to be significantly more active than traditional iron-based catalysts (Hansen et al. 2001, 2002b; Kowalczyk et al. 1996). The addition of barium as promoter increased the integral reaction by more than a factor of 10. Hence, obtaining insight into the role of the promoter phase could provide valuable insight into workings of this catalyst system.

When imaged in high vacuum at room temperature, the surface of the ruthenium nanoparticles was covered by a layered structure identified as hexagonal boron nitride, a strong indication of strong metal support interactions (SMSI) (Tauster et al. 1978; Tauster 1987). This layer entirely disguised the surface structure of the metal nanoparticles, see Fig. 8.3a, b. When exposed to a reactive environment consisting of a 3:1 mixture of H_2 and N_2 in the ETEM at a total pressure of about 500 Pa at ca. 550 °C, the surface layer was removed exposing the surface of the metal particles, see Fig. 8.3c, d. A similar surface coverage was observed by Kowalczyk and coworkers for ruthenium supported on carbon (Kowalczyk et al. 1999). After treatment in H_2/N_2, the surfaces of the metal particles revealed a periodic structure, see Fig. 8.3d, which by EELS was shown to contain barium. As the promoter phase was observed on the surface of the active metal particles, the promotional effect was believed to be of electronic nature. This was, however, contested by other studies (Szmigiel et al. 2002; Raróg et al. 2000).

The striking difference in surface structure from vacuum to a reactive environment shows the significance of imaging catalytic metal nanoparticles under conditions resembling the operating environment if the true nature of the active site is to be unraveled. Furthermore, it stresses the importance of imaging catalysts under reactive environments if any information about active sites is to be obtained.

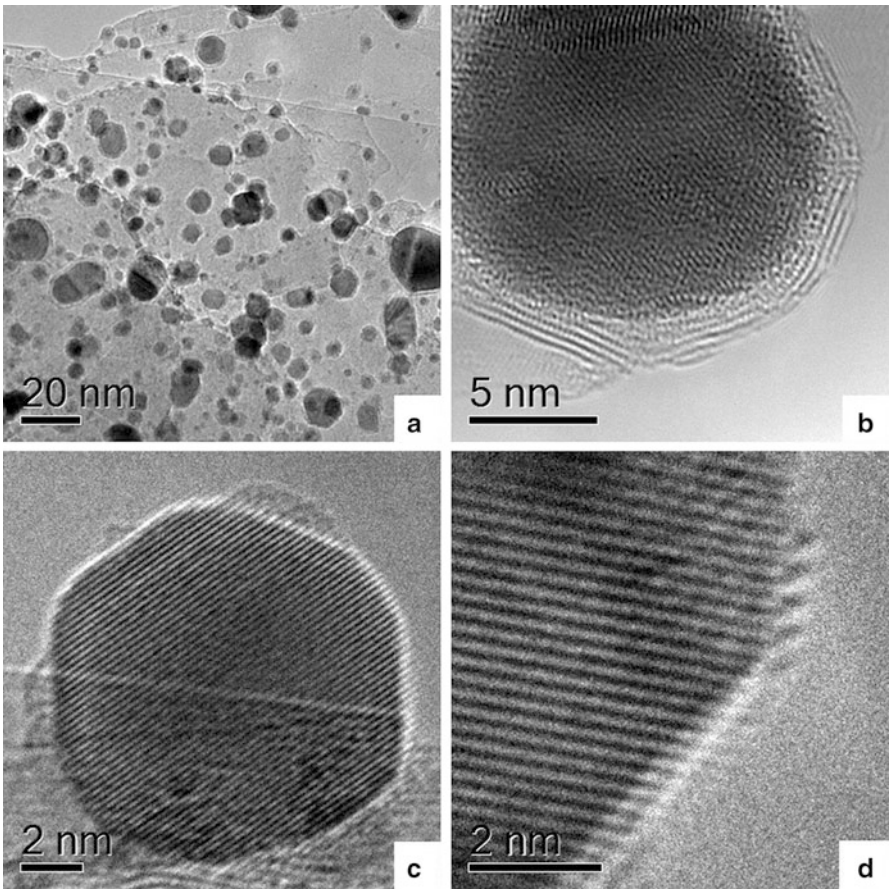

Fig. 8.3 Ruthenium nanoparticles supported on boron nitride. In vacuum (**a**, **b**), all particles are encapsulated in boron nitride layers. Ruthenium nanoparticles supported on boron nitride in 3:1 H_2/N_2 at 450 °C (**c**, **d**) the surfaces are exposed to the gas phase. Reproduced from (Hansen et al. 2001). Copyright 2001 American Association for the Advancement of Science

8.3.4 Photocatalysis

Photocatalysis, where light irradiation provides most of the energy for a reaction, has great potential for solar fuels (Kudo and Miseki 2009). In order to understand structure-reactivity relations at the atomic level, it is necessary to introduce light as a stimulus in the ETEM in addition to a gaseous phase, typically water vapor.

Allowing sample irradiation with light has been accomplished in two distinct ways. Either light has been coupled to the sample via a port on the objective lens of the microscope (Miller and Crozier 2011) or through the barrel of the sample holder (Cavalca et al. 2012; Shindo et al. 2009). Each approach comes with its own

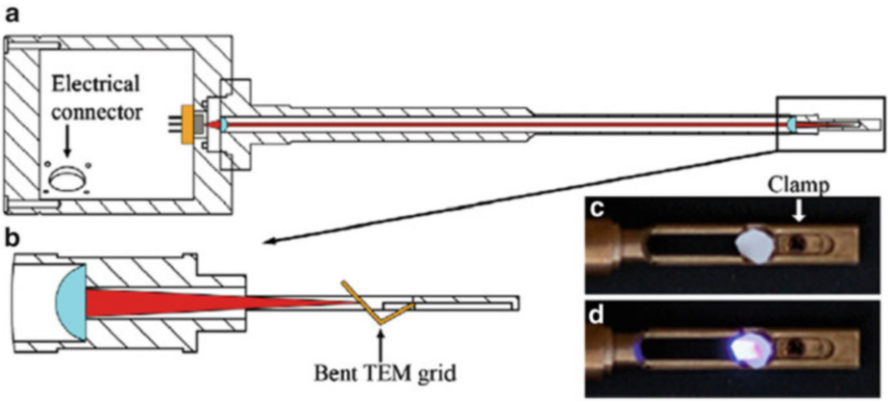

Fig. 8.4 Schematic cross-sectional view of the lens-based specimen holder. (**a**) The feedthrough on the left hosts a laser diode, which is connected through a mini-DIN connector installed in the lateral port. Two lenses (shown in *blue*), selected for the chosen laser wavelength, collimate and focus the light onto the sample. (**b**) A close-up cross-sectional side view of the tip. The sample (shown in *yellow*) is bent in order to allow it to be exposed to both light and electron beams. (**c**, **d**). Photographs of the tip with the illumination off and on, respectively (Cavalca et al. 2012)

advantages and complexities. Whereas the former approach allows for using different holder with additional functionality, e.g., heating, the latter construction offers the possibility of compatibility with different microscopes. Figure 8.4 shows the design of a holder with an integrated lens focusing the light onto the sample. A laser diode is fitted into the housing of the holder. In a similar design, optical fibers are inserted into the barrel of the holder guiding the light all the way to the sample. When inserting the fibers through the objective lens of the microscope, special considerations have to be made regarding the termination of the optical fiber inside the microscope in order to achieve an even illumination of the sample.

Using in situ illumination, Cavalca et al. studied the evolution of cuprous oxide in an aqueous atmosphere. Cu_2O nanocubes in the range 100–200 nm were dispersed onto a lacey carbon film on a gold TEM grid. The sample was characterized using TEM, electron diffraction, and EELS prior to exposure to water vapor and light. Figure 8.5 shows the evolution via the three techniques. All data clearly indicates a reduction from oxide to metal during light illumination.

Miller and Crozier adapted and ETEM to include an optical fiber into the sample region via the microscope column (Miller and Crozier 2011). Using this setup, Zhang et al. studied the amorphization of anatase titanium dioxide, a stable catalyst for water splitting. In their investigation, an amorphous layer formed on top of initially crystalline facets (Zhang et al. 2013b). Figure 8.6 shows a titania particle exposed to light and water vapor for 12 h showing a disordered layer on the (101) and (002) facets. The process was found to be self-limiting as the thickness of the layer did not increase after prolonged exposure to light and water vapor. This is in agreement with the stability of the catalyst.

ETEM compatible light illumination has been developed, and interested readers should see the references (Cavalca et al. 2012, 2013; Miller and Crozier 2011, 2012, 2013).

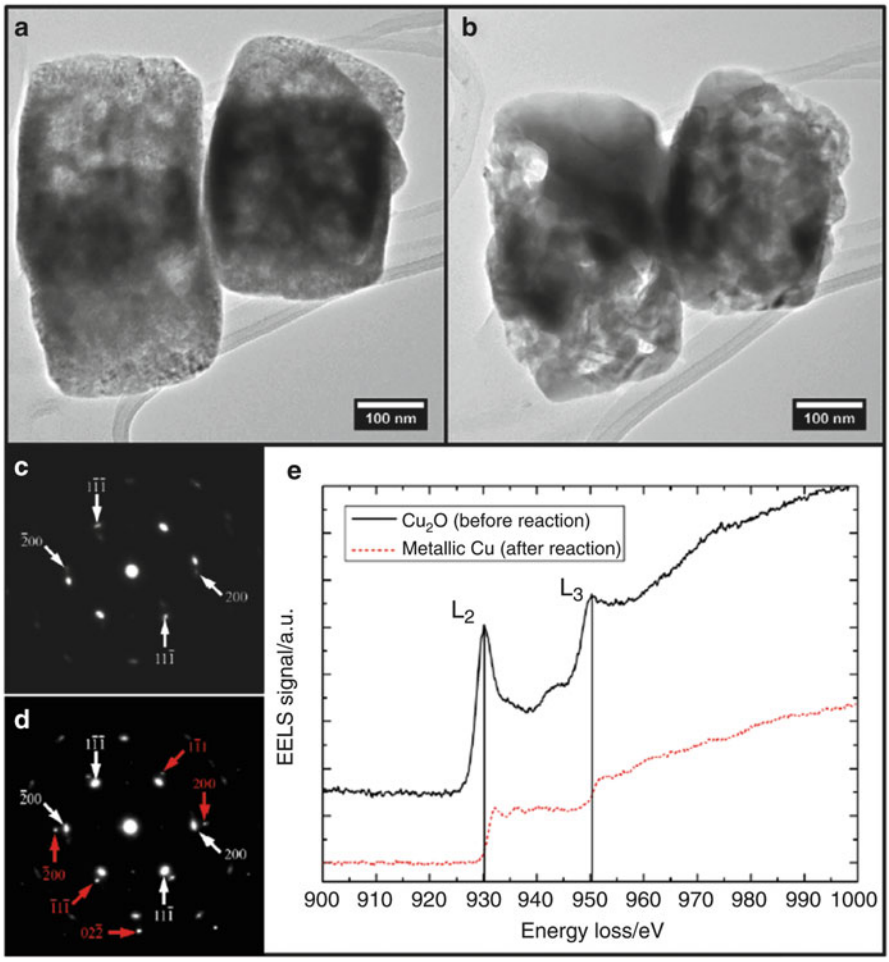

Fig. 8.5 (**a**, **b**) Bright-field TEM images of Cu_2O nanocubes before and after reaction, respectively, showing changes in particle shape and morphology (Cavalca et al. 2012). No significant damage to the supporting carbon film was observed. The growth of large single crystals of Cu is observed. (**c**, **d**) Selected area diffraction patterns in the [011] zone axis, indexed for Cu_2O (**c**) and for both Cu_2O and Cu (**d**). The area sampled by the selected area aperture is 400 nm in diameter and encompasses at least two of the particles shown in (**a**, **b**). After the reaction, (**d**) contains spots representative of metallic copper, labeled in *red*. Spots from Cu_2O are still present as some portions of the particles are not completely reduced. (**e**) Electron energy-loss spectra of the same nanocubes. The *upper curve* is offset vertically for ease of comparison. The positions of the peaks of the L_2 and L_3 EELS edges are indicated by the *vertical black lines*

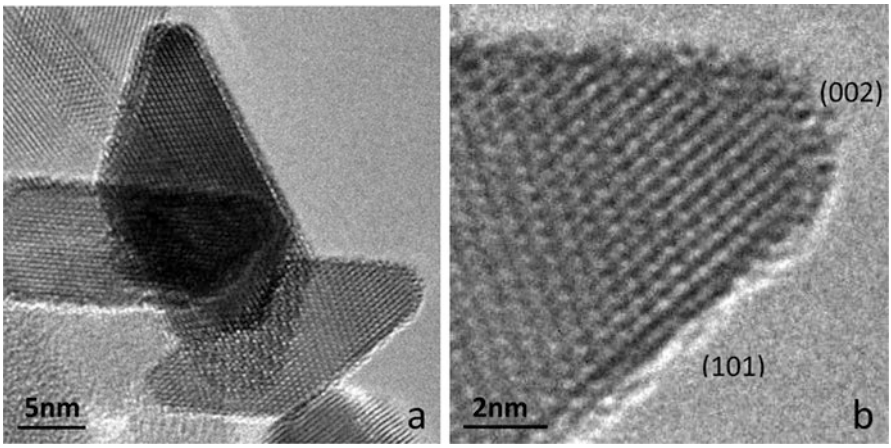

Fig. 8.6 (**a**) Fresh anatase particles after 40 h in H_2O gas at 150 °C, light exposure 12 h; (**b**) magnified images of the (101) and (002) surfaces after illumination. The image was taken in 20 s including adjusting the focus (Zhang et al. 2013b)

8.4 Catalyst Deactivation

8.4.1 Dynamic Studies: Growth and Oxidation of Carbon Structures

Catalyzed growth of extended carbon nanofiber structures in the form of either filaments or tubes have been a major point of interest for decades. Before the constructive use of carbon nanotubes in materials science, the formation of carbon nanofiber structures has been acknowledged as a severe problem in heterogeneous catalysis. For instance, in nickel-based steam-reforming catalysts, the growth of carbon nanofibers resulting from low H_2O/C ratio or high temperature can have catastrophic effects (Rostrup-Nielsen and Christiansen 2011). When fibers grow inside catalyst pellets, they can break up the pellet structuring leaving granulates blocking the reactor resulting in a high pressure drop (Rostrup-Nielsen 1975).

Helveg et al. studied the formation of fibrous carbon structures in a nickel-based steam-reforming catalyst using environmental TEM (Helveg et al. 2004). In a 1:1 mixture of hydrogen and methane, growth of both carbon filaments or whiskers and carbon nanotubes (CNTs) was observed. Figure 8.7 illustrates the dynamical behavior of the Ni catalysts during CNT growth. Based on the experimental observation of the growth process and modelling by density functional theory (DFT), the authors concluded that individual graphene layers of the carbon filaments were formed at step edges as the carbon atoms bind more strongly here. Details on the experiment are described by Helveg et al. (2004) and corresponding supplementary movies showing the growth.

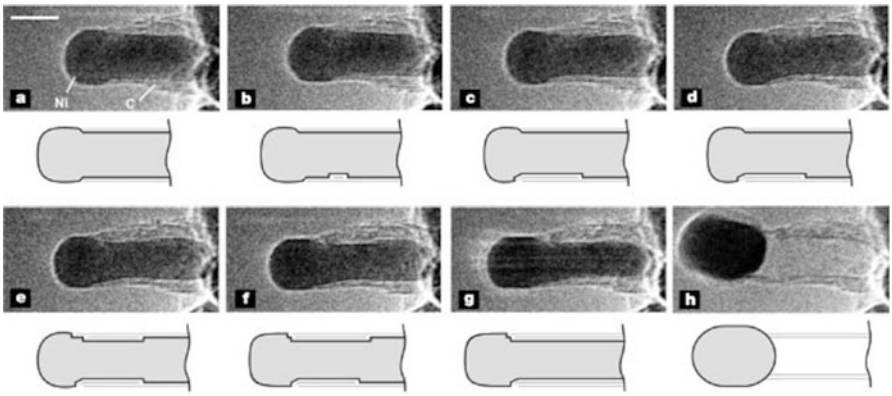

Fig. 8.7 Image sequence of a growing carbon nanofiber illustrating an elongation/contraction process. Mono-atomic Ni steps are found to be the point of formation for the carbon layers (guide-to-the-eye drawings are included in the figure). The images are acquired in situ with CH_4:H_2=1:1 at 210 Pa with the sample heated to 536 °C. Reproduced from (Helveg et al. 2004). Copyright 2004 Nature Publishing Group (Helveg et al. 2004)

With stricter demands on emission control being enforced worldwide, oxidation of particulate matter from particularly diesel engines is a topic of increasing interest (van Setten et al. 2001). Simonsen et al. studied the oxidation of soot over a ceria catalyst (Simonsen et al. 2008) for vehicle emission control with emphasis on the soot-ceria interface under oxidizing conditions. As model soot, 30 nm carbon black particles were used. The study concluded that the oxidation occurs solely at the soot-ceria interface. A motion of the particles towards the interface, which established a continuous interface and an efficient reaction point, accompanied the oxidation of soot.

8.4.2 Sintering of Supported Metal Catalysts

Sintering or growth of nanoparticles is a deactivation route that plagues supported metal catalysis (Sehested 2006). The phenomenon has been studied at great length using TEM under a controlled atmosphere from the time the technique became available (Baker et al. 1974). More recent studies include both model systems (Simonsen et al. 2010, 2011; Benavidez et al. 2012) as well as technical catalysts (Hansen 2006; Hansen et al. 2013; Liu et al. 2004).

Two mechanisms of mass transfer are suggested to be responsible for sintering of metal nanoparticles. One mechanism suggests that atomic species or small entities can migrate from smaller to larger particles due to a difference in chemical potential; this is known as Ostwald ripening (OR). The other mechanism is particle migration and coalescence (PMC), where particles migrate on the substrate and coalesce into single particles as they encounter each other. Both mechanisms play a

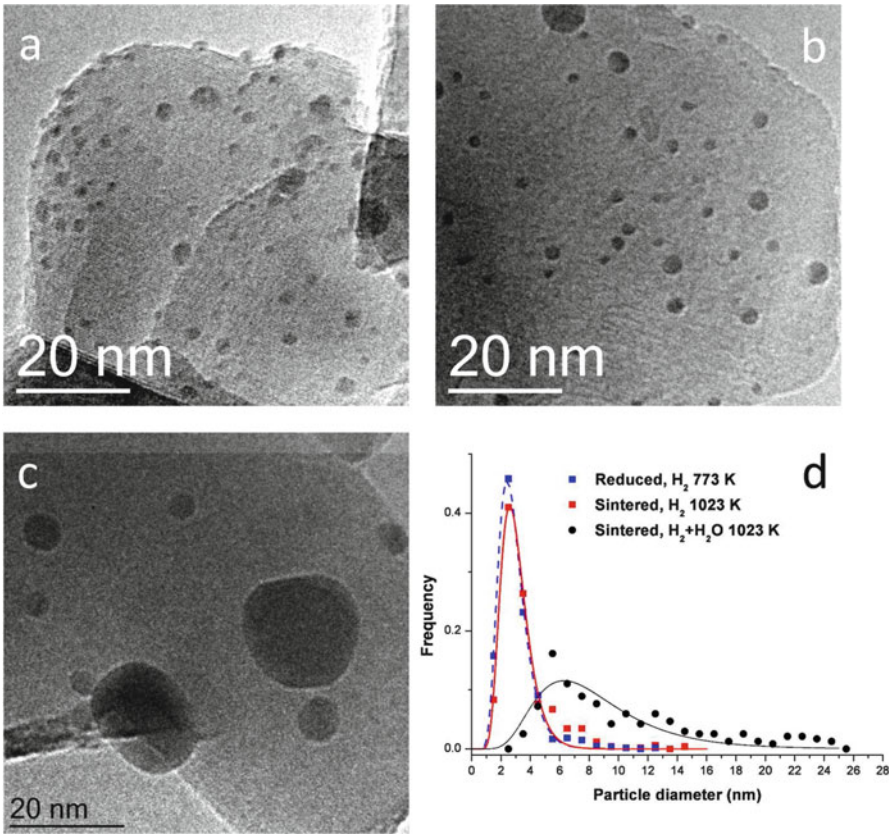

Fig. 8.8 TEM images of a $Ni/MgAl_2O_4$ sample. (**a**) After reduction in 300 Pa H_2 at 500 °C; (**b**) after sintering for 5 h in 200 Pa H_2 at 750 °C; (**c**) after sintering for 5 h in 200 Pa H_2 and 200 Pa H_2O at 750 °C; (**d**) particle size distributions for the three cases. Reproduced from (Hansen et al. 2013). Copyright 2013 American Chemical Society

role in industrial catalysis, the dominant mechanism being determined by the reaction conditions. Traditionally, the shape of the particle size distribution after a given time on stream has been used to determine the mechanism of sintering. A tail on the small diameter side of the mean size indicated an OR mechanism, whereas a tail on the large diameter side of the mean indicates growth by PMC (Wynblatt and Gjostein 1975; Granqvist and Buhrman 1975).

Figure 8.8 shows images and size distributions of spinel-supported nickel nanoparticles determined from TEM images. First, the sample was reduced in 300 Pa H_2 at 500 °C (Fig. 8.8a), and then exposed to the sintering environment, 200 Pa H_2 at 750 °C (Fig. 8.8b) and 200 Pa H_2 and 200 Pa H_2O at 750 °C (Fig. 8.8c) for 5 h. The particle size distributions after reduction and after sintering determined from a set of TEM images are shown in Fig. 8.8d. Both distributions after sintering show a tail on the large diameter side of the mean indicating that the growth

occurred via PMC and a strong effect of atmosphere composition is observed. In order to further document the sintering mechanism, the particles were imaged during exposure to the sintering environments (Hansen et al. 2013). Based on these observations along with observation of the initial exposure to a reactive environment (DeLaRiva et al. 2013; Challa et al. 2011), Hansen et al. suggested that the sintering of supported metal nanoparticles could be divided into three phases (Hansen et al. 2013). In phase 1, a rapid decrease of activity is observed, and sintering is dominated by OR. During this stage, the catalyst reaches its operating temperature and the metal particles attain their equilibrium shape. In phase 2, sintering slows down but particles still grow in size, mainly via particle migration. Phase 3 represents the stable operation of the catalyst; the active particles have reached a size, where migration is very slow.

The same authors have also investigated the phenomenon of anomalous particle growth (Benavidez et al. 2012). Here, some particles grow to sizes significantly larger than the ensemble mean size. The phenomenon was already described in the mid 1970s by Wynblatt and Gjostein (1975). Platinum particles were physically deposited on a silicon oxide film and investigated in the ETEM. The sample was exposed to a flow of oxygen at 560 Pa, and the temperature was increased to 550 °C. Sets of images were acquired in intervals over 10 h while keeping the electron beam off between image acquisition in order to minimize the electron exposure of the sample, see Fig. 8.9. After prolonged exposure to the sintering conditions, particles with a diameter considerably larger than the mean started to evolve. The emergence of these particles does not result in a significant shift in the particle size distribution (Fig. 8.10).

Traditionally, the migration of nanoparticles has been a strong function of the particle size (r^{-4} dependence). Whereas such a behavior may be true on a perfectly flat substrate, other observations have been made recently. Hansen et al. studied the mobility of nickel particles on a magnesium aluminum spinel substrate. Here, particles were observed to migrate be creeping along steps on the support. However, contrary to conventional knowledge, the smallest particles were rarely the most mobile. Larger particles were observed to be more mobile and coalesce with

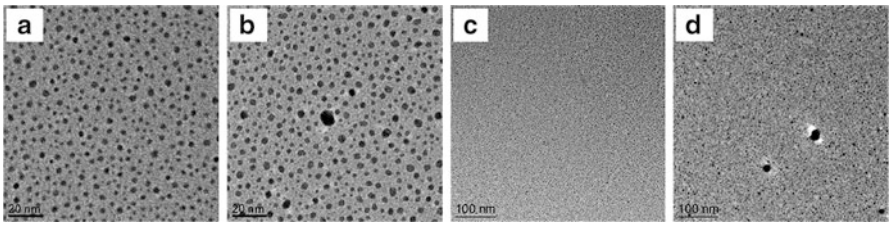

Fig. 8.9 Platinum NPs supported on SiO_2/Si_3N_4 acquired in 560 Pa O_2 at 550 °C. Panels (**a**, **b**) are acquired after 30 min and panels (**c**, **d**) after 10 h. Panels (**a**, **b**) show high magnification images recorded after 30 min and 10 h, respectively, and used for determination of PSDs. Panels (**c**, **d**) show medium magnification images recorded after the same times. At medium magnification, panels (**c**, **d**), a larger field of view is captured and the appearance of anomalously large particles is evident (Benavidez et al. 2012)

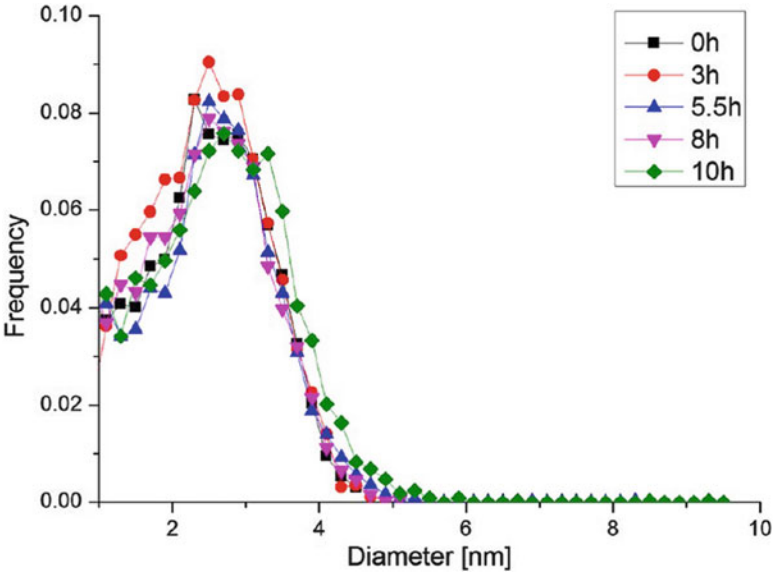

Fig. 8.10 PSDs determined after 0, 3, 5.5, 8, and 10 h, respectively, from images acquired at high magnification. The distributions appear very similar up to 8 h after which a slight shift to larger particles is observed. The bin size is 0.2 nm (Benavidez et al. 2012)

smaller particles on their route. The smallest particles appear to be stable whereas the larger particles migrate, see Fig. 8.11. These observations indicate that the structure of the support may play a significant role in stabilizing catalytic nanoparticles.

Even though sintering in practice is challenging to control, knowledge of the governing processes is crucial if more sintering stable catalysts are to be developed. Modifications of the support material creating more anchoring sites is one possibility that may limit particle migration or even reduce migration speeds of single atoms or small clusters reducing Ostwald ripening. Such materials engineering could greatly benefit society.

8.4.3 Fuel Cells

Fuel cells are one of the most promising technologies for decentralized energy production. They exist in various forms operating at various temperatures. The class of fuel cells known as solid oxide fuel cells (SOFC) are candidates for power production up to a few megawatts. The name stems from the use of a solid oxide as the electrolyte transporting the negatively charged oxygen ions from the cathode to the anode. The anode of an SOFC typically consists of nickel oxide and yttria-stabilized zirconia (YSZ). It is synthesized by sintering NiO particles with YSZ

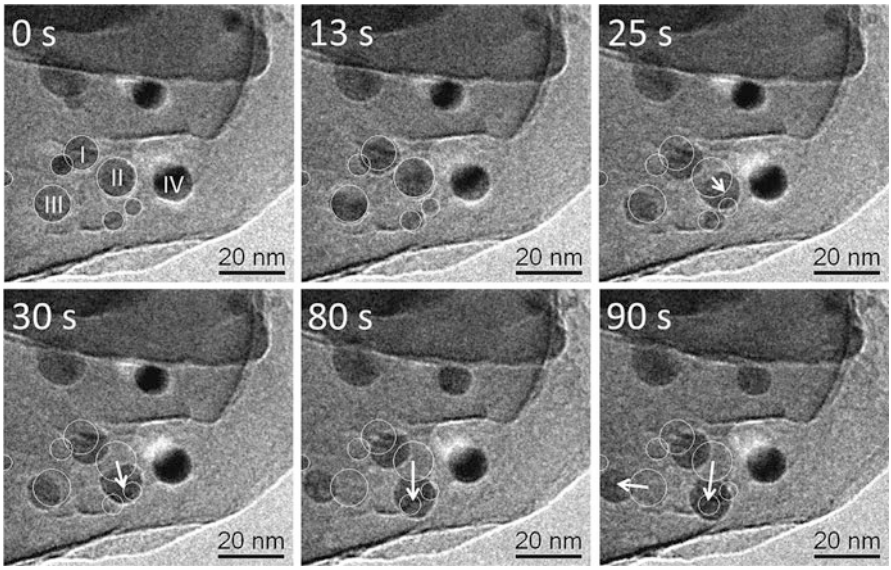

Fig. 8.11 TEM images of $Ni/MgAl_2O_4$ catalyst. This is an image sequence acquired in 200 Pa H_2O and 200 Pa H_2 at 750 °C. Individual frames have been aligned to make it easier to see the motion of individual nanoparticles and to allow us to track these particles. The frames are acquired at 0, 13, 25, 30, 80, and 90 s. The *white circles* indicate the initial positions of the particles and four particles that survived at the end of the treatment are indicated with numbers I–IV. *Arrows* show the particle mobility seen in the next frame. The image sequence shows that the larger particles are more mobile than the smaller particles, and the particles appear to nucleate preferentially at steps on the support (Hansen et al. 2013)

followed by a reduction process. During the reduction, pores are formed in the anode-enhancing gas permeability. During standard operating conditions, the nickel is kept in the reduced state. However, various types of failures including seal leakage and uncontrolled shut downs may result in reoxidation.

Jeangros et al. studied the reduction and reoxidation of a slice of an SOFC using environmental transmission electron microscopy (Jeangros et al. 2010). The slice was prepared using focused ion beam (FIB) and was attached to a TEM grid for mounting in a heating holder. First, the samples were exposed to 140 Pa of flowing hydrogen, and the temperature was ramped up to 200 °C. After allowing 30 min for stabilization, after which the temperature was further increased to first 300 °C in two steps and then to 500 °C in 10 °C steps. From 300 °C and onwards, bright-field images, diffraction patterns, and EELS were acquired in order to monitor the oxidation state of nickel, see Fig. 8.12. The reduction was observed to initiate as nanovoids at the NiO/YSZ interfaces starting at 340 °C. At 420 °C, the free surfaces of the NiO grains start to reduce and the porosity fills the entire NiO grains. After reaching 500 °C, the temperature was maintained for 2 h and then ramped down to room temperature, still in flowing H_2. After reaching room temperature, the H_2 was evacuated from the ETEM and oxygen was introduced at a pressure of 320 Pa and a

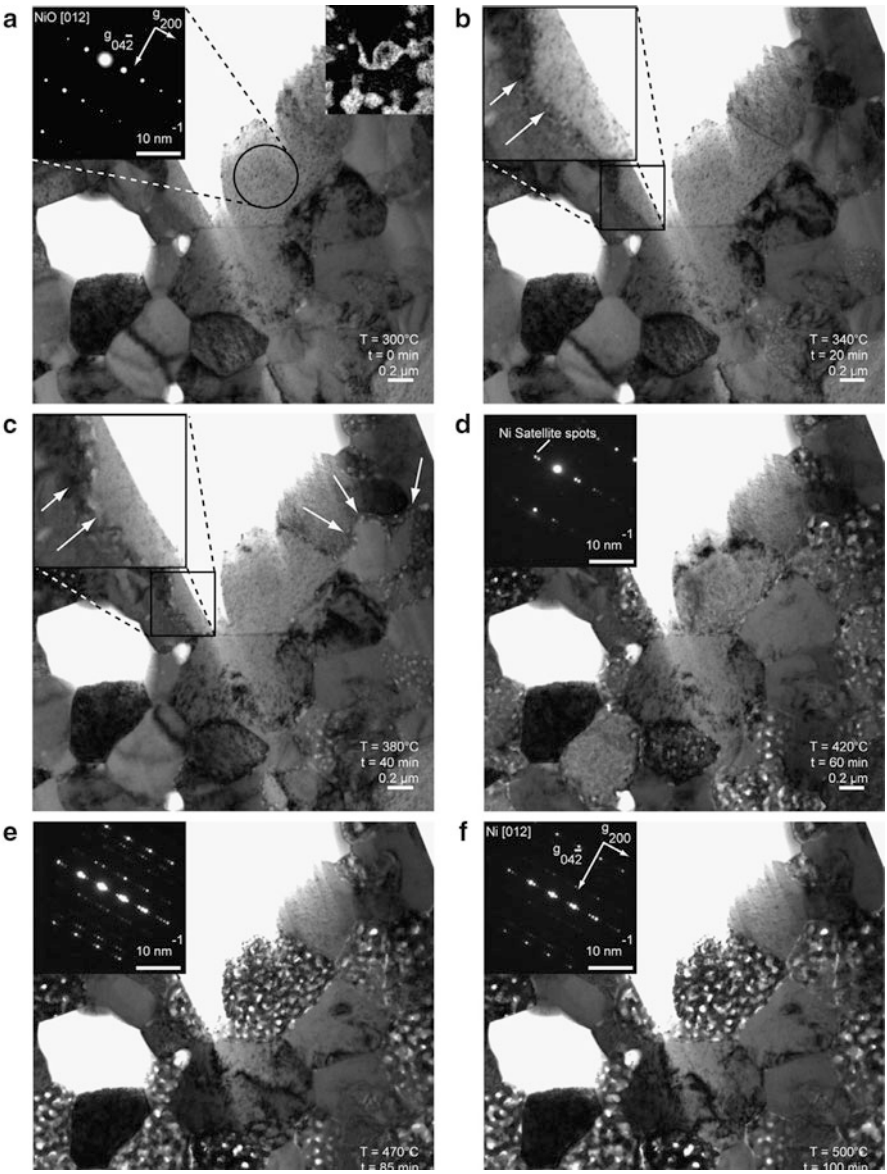

Fig. 8.12 Bright-field TEM images acquired during in situ reduction of a NiO/YSZ anode precursor in 140 Pa of H_2. Higher magnification images, diffraction patterns, and a nickel map obtained using energy-filtered TEM are shown as *insets*. The *arrows* in (**b**, **c**) show the nanovoids (Jeangros et al. 2010)

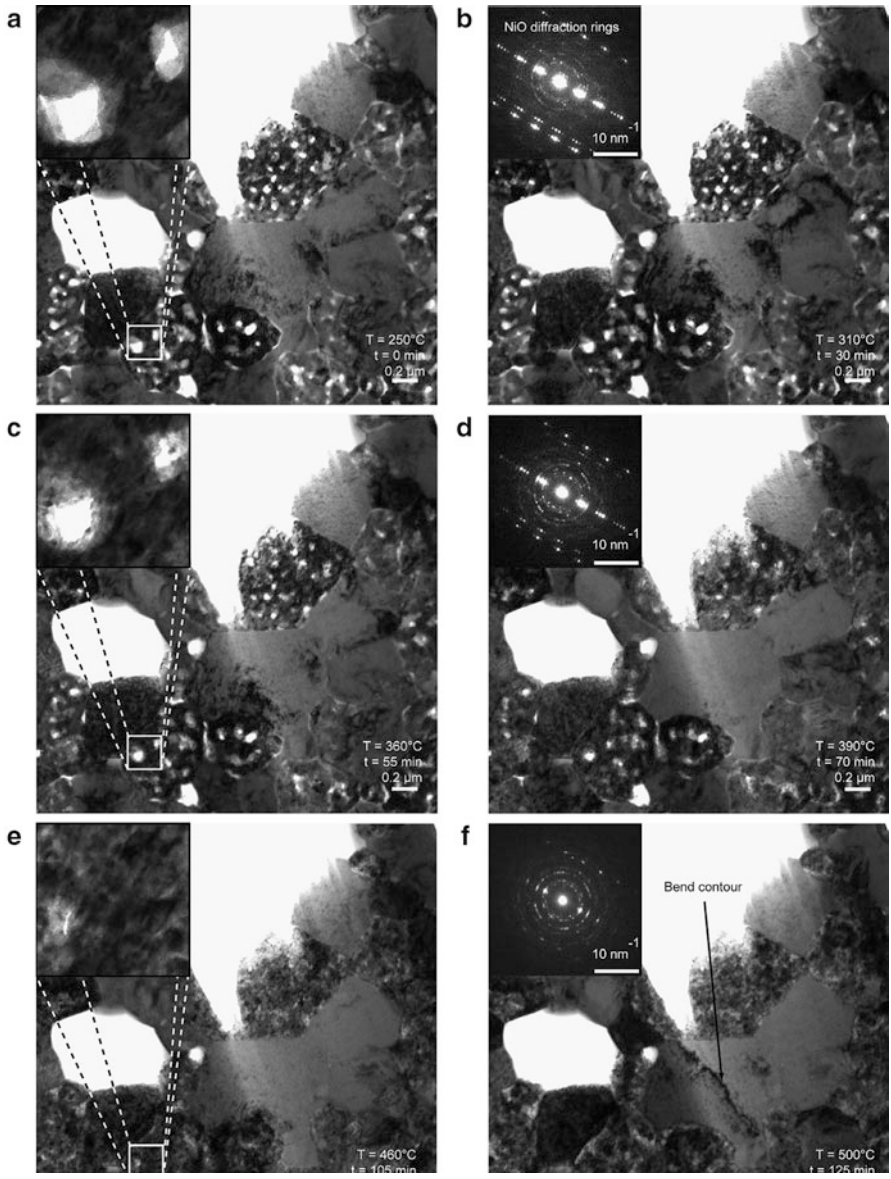

Fig. 8.13 Bright-field TEM images acquired during in situ reoxidation in 320 Pa O_2. Higher magnification images and diffraction patterns are shown as *insets* (Jeangros et al. 2010)

similar temperature increase and data acquisition as during reduction was performed, see Fig. 8.13. During reoxidation, the voids formed during reduction are filled with polycrystalline nickel oxide. Contrary to the reduction process, the reoxidation process occurs uniformly throughout the nickel grains starting at ca. 290 °C.

In this study, results obtained from ETEM support previous experimental observations (Waldbillig et al. 2005) and theoretical predictions (Jeangros et al. 2010). The results were further corroborated by investigations of oxidation properties of nickel particles under similar conditions (Jeangros et al. 2014).

8.5 Conclusions

The investigation of catalysts in a reactive environment can be a daunting feat scientifically as well as technically. Catalysts are dynamic entities and their state and structure changes with their surroundings and over time. ETEM provides a powerful tool for imaging samples at the atomic scale with simultaneous acquisition of spectroscopic information, all in a simulated working environment. Having this tool in the toolbox provides information on the local level that can ultimately dictate the development of the next generation of catalysts and functional materials when combined with other more globally probing characterization and analysis tools.

References

T. Akita, P. Lu, S. Ichikawa, K. Tanaka, M. Haruta, Analytical TEM study on the dispersion of Au nanoparticles in Au/TiO_2 catalyst prepared under various temperatures. Surf. Interface Anal. **31**, 73–78 (2001)

T. Akita, M. Kohyama, M. Haruta, Electron microscopy study of gold nanoparticles deposited on transition metal oxides. Acc. Chem. Res. **46**, 1773–1782 (2013)

T.S. Askgaard, J.K. Norskov, C.V. Ovesen, P. Stoltze, A kinetic-model of methanol synthesis. J. Catal. **156**, 229–242 (1995)

R.T.K. Baker, P.S. Harris, R.B. Thomas, Direct observation of particle mobility on a surface in a gaseous environment. Surf. Sci. **46**, 311–316 (1974)

A.D. Benavidez, L. Kovarik, A. Genc, N. Agrawal, E.M. Larsson, T.W. Hansen, A.M. Karim, A.K. Datye, Environmental transmission electron microscopy study of the origins of anomalous particle size distributions in supported metal catalysts. ACS Catal. **2**, 2349–2356 (2012)

M. Boudart, Turnover rates in heterogeneous catalysis. Chem. Rev. **95**, 661–666 (1995)

S.H. Brodersen, U. Gronbjerg, B. Hvolbaek, J. Schiotz, Understanding the catalytic activity of gold nanoparticles through multi-scale simulations. J. Catal. **284**, 34–41 (2011)

M. Cabie, S. Giorgio, C.R. Henry, M.R. Axet, K. Philippot, B. Chaudret, Direct observation of the reversible changes of the morphology of Pt nanoparticles under gas environment. J. Phys. Chem. C **114**, 2160–2163 (2010)

A. Carlsson, A. Puig-Molina, T.V.W. Janssens, New method for analysis of nanoparticle geometry in supported fee metal catalysts with scanning transmission electron microscopy. J. Phys. Chem. B **110**, 5286–5293 (2006)

F. Cavalca, A.B. Laursen, B.E. Kardynal, R.E. Dunin-Borkowski, S. Dahl, J.B. Wagner, T.W. Hansen, In situ transmission electron microscopy of light-induced photocatalytic reactions. Nanotechnology **23**, 075705 (2012)

F. Cavalca, A.B. Laursen, J.B. Wagner, C.D. Damsgaard, I. Chorkendorff, T.W. Hansen, Light-induced reduction of cuprous oxide in an environmental transmission electron microscope. ChemCatChem **5**, 2667–2672 (2013)

S.R. Challa, A.T. Delariva, T.W. Hansen, S. Helveg, J. Sehested, P.L. Hansen, F. Garzon, A.K. Datye, Relating rates of catalyst sintering to the disappearance of individual nanoparticles during Ostwald ripening. J. Am. Chem. Soc. **133**, 20672–20675 (2011)

S. Chenna, P.A. Crozier, Operando transmission electron microscopy: a technique for detection of catalysis using electron energy-loss spectroscopy in the transmission electron microscope. ACS Catal. **2**, 2395–2402 (2012)

I. Chorkendorff, J.W. Niemantsverdriet, *Concepts of Modern Catalysis and Kinetics* (Wiley-VCH, Weinheim, 2003)

A.K. Datye, Electron microscopy of catalysts: recent achievements and future prospects. J. Catal. **216**, 144–154 (2003)

A.T. DeLaRiva, T.W. Hansen, S.R. Challa, A.K. Datye, In situ transmission electron microscopy of catalyst sintering. J. Catal. **308**, 291–305 (2013)

D.J. Flannigan, A.H. Zewail, 4D Electron microscopy: principles and applications. Acc. Chem. Res. **45**, 1828–1839 (2012)

P.L. Gai, E.D. Boyes, S. Helveg, P.L. Hansen, S. Giorgio, C.R. Henry, Atomic-resolution environmental transmission electron microscopy for probing gas-solid reactions in heterogeneous catalysis. MRS Bull. **32**, 1044–1050 (2007)

S. Giorgio, M. Cabie, C.R. Henry, Dynamic observations of Au catalysts by environmental electron microscopy. Gold Bull. **41**, 167–173 (2008)

C.G. Granqvist, R.A. Buhrman, Statistical-model for coalescence of islands in discontinuous films. Appl. Phys. Lett. **27**, 693–694 (1975)

J.D. Grunwaldt, A.M. Molenbroek, N.Y. Topsøe, H. Topsøe, B.S. Clausen, In situ investigations of structural changes in Cu/ZnO catalysts. J. Catal. **194**, 452–460 (2000)

J.D. Grunwaldt, J.B. Wagner, R.E. Dunin-Borkowski, Imaging catalysts at work: a hierarchical approach from the macro- to the meso- and nano-scale. ChemCatChem **5**, 62–80 (2013)

B. Hammer, J.K. Nørskov, Why gold is the noblest of all the metals. Nature **376**, 238 (1995)

T.W. Hansen, *Sintering and Particle Dynamics in Supported Metal Catalysts, in Department of Chemistry* (Lyngby, Technical University of Denmark, 2006)

T.W. Hansen, J.B. Wagner, Environmental transmission electron microscopy in an aberration-corrected environment. Microsc. Microanal. **18**, 684–690 (2012)

T.W. Hansen, J.B. Wagner, Catalysts under controlled atmospheres in the transmission electron microscope. ACS Catal. **4**, 1673–1685 (2014)

T.W. Hansen, J.B. Wagner, P.L. Hansen, S. Dahl, H. Topsøe, C.J.H. Jacobsen, Atomic-resolution in situ transmission electron microscopy of a promoter of a heterogeneous catalyst. Science **294**, 1508–1510 (2001)

P.L. Hansen, J.B. Wagner, S. Helveg, J.R. Rostrup-Nielsen, B.S. Clausen, H. Topsøe, Atom-resolved imaging of dynamic shape changes in supported copper nanocrystals. Science **295**, 2053–2055 (2002a)

T.W. Hansen, P.L. Hansen, S. Dahl, J.H. Jacobsen, Support effect and active sites on promoted ruthenium catalysts for ammonia synthesis. Catal. Lett. **84**, 7–12 (2002b)

P.L. Hansen, S. Helveg, A.K. Datye, Atomic-scale imaging of supported metal nanocluster catalysts in the working state. Adv. Catal. **50**, 77–95 (2006)

T.W. Hansen, A.T. Delariva, S.R. Challa, A.K. Datye, Sintering of catalytic nanoparticles: particle migration or Ostwald ripening? Acc. Chem. Res. **46**, 1720–1730 (2013)

M. Haruta, N. Yamada, T. Kobayashi, S. Iijima, Gold catalysts prepared by coprecipitation for low-temperature oxidation of hydrogen and of carbon-monoxide. J. Catal. **115**, 301–309 (1989)

M. Haruta, S. Tsubota, T. Kobayashi, H. Kageyama, M.J. Genet, B. Delmon, Low-temperature oxidation of CO over gold supported on TiO_2, alpha-Fe_2O_3, and Co_3O_4. J. Catal. **144**, 175–192 (1993)

S. Helveg, C. Lopez-Cartes, J. Sehested, P.L. Hansen, B.S. Clausen, J.R. Rostrup-Nielsen, F. Abild-Pedersen, J.K. Nørskov, Atomic-scale imaging of carbon nanofibre growth. Nature **427**, 426–429 (2004)

K. Honkala, A. Hellman, I.N. Remediakis, A. Logadottir, A. Carlsson, S. Dahl, C.H. Christensen, J.K. Norskov, Ammonia synthesis from first-principles calculations. Science **307**, 555–558 (2005)

C.J.H. Jacobsen, Boron nitride: a novel support for ruthenium-based ammonia synthesis catalysts. J. Catal. **200**, 1–3 (2001)

T.V.W. Janssens, A. Carlsson, A. Puig-Molina, B.S. Clausen, Relation between nanoscale Au particle structure and activity for CO oxidation on supported gold catalysts. J. Catal. **240**, 108–113 (2006)

Q. Jeangros, A. Faes, J.B. Wagner, T.W. Hansen, U. Aschauer, J. Van Herle, A. Hessler-Wyser, R.E. Dunin-Borkowski, In situ redox cycle of a nickel-YSZ fuel cell anode in an environmental transmission electron microscope. Acta Mater. **58**, 4578–4589 (2010)

Q. Jeangros, T.W. Hansen, J.B. Wagner, R.E. Dunin-Borkowski, C. Hebert, J. Van Herle, A. Hessler-Wyser, Oxidation mechanism of nickel particles studied in an environmental transmission electron microscope. Acta Mater. **67**, 362–372 (2014)

Z. Kowalczyk, S. Jodzis, J. Sentek, Studies on kinetics of ammonia synthesis over ruthenium catalyst supported on active carbon. Appl. Catal. A **138**, 83–91 (1996)

Z. Kowalczyk, S. Jodzis, W. Raróg, J. Zieliński, J. Pielaszek, A. Presz, Carbon-supported ruthenium catalyst for the synthesis of ammonia. The effect of the carbon support and barium promoter on the performance. Appl. Catal. A **184**, 95–102 (1999)

G. Kresse, J. Hafner, Ab-initio molecular dynamics for open-shell transition metals. Phys. Rev. B **48**, 13115–13118 (1993)

A. Kudo, Y. Miseki, Heterogeneous photocatalyst materials for water splitting. Chem. Soc. Rev. **38**, 253–278 (2009)

R.J. Liu, P.A. Crozier, C.M. Smith, D.A. Hucul, J. Blackson, G. Salaita, In situ electron microscopy studies of the sintering of palladium nanoparticles on alumina during catalyst regeneration processes. Microsc. Microanal. **10**, 77–85 (2004)

B.K. Miller, P.A. Crozier, Visible and UV irradiation of ETEM samples for in-situ studies of photocatalysts. Microsc. Microanal. **17**(Suppl 2), 472–473 (2011)

B.K. Miller, P.A. Crozier, In situ visible and UV illumination of ETEM samples. Microsc. Microanal. **18**(Suppl 2), 1074–1075 (2012)

B.K. Miller, P.A. Crozier, System for in situ UV-visible illumination of environmental transmission electron microscopy samples. Microsc. Microanal. **19**, 461–469 (2013)

L.M. Molina, S. Lee, K. Sell, G. Barcaro, A. Fortunelli, B. Lee, S. Seifert, R.E. Winans, J.W. Elam, M.J. Pellin, I. Barke, V. von Oeynhausen, Y. Lei, R.J. Meyer, J.A. Alonso, A.F. Rodriguez, A. Kleibert, S. Giorgio, C.R. Henry, K.H. Meiwes-Broer, S. Vajda, Size-dependent selectivity and activity of silver nanoclusters in the partial oxidation of propylene to propylene oxide and acrolein: a joint experimental and theoretical study. Catal. Today **160**, 116–130 (2011)

W. Raróg, Z. Kowalczyk, J. Sentek, D. Skladanowski, J. Zieliński, Effect of K, Cs and Ba on the kinetics of NH_3 synthesis over carbon-based ruthenium catalysts. Catal. Lett. **68**, 163–168 (2000)

J.R. Rostrup-Nielsen, *Steam Reforming Catalysts* (Danish Technical Press, Copenhagen, 1975)

J. Rostrup-Nielsen, L.J. Christiansen, in *Concepts in Syngas Manufacture*, ed. by G.J. Hutchings. Catalytic Science Series, vol. 10 (Imperial College Press, London, 2011)

J. Sehested, Four challenges for nickel steam-reforming catalysts. Catal. Today **111**, 103–110 (2006)

D. Shindo, K. Takahashi, Y. Murakami, K. Yamazaki, S. Deguchi, H. Suga, Y. Kondo, Development of a multifunctional TEM specimen holder equipped with a piezodriving probe and a laser irradiation port. J. Electron. Microsc. **58**, 245–249 (2009)

S.B. Simonsen, S. Dahl, E. Johnson, S. Helveg, Ceria-catalyzed soot oxidation studied by environmental transmission electron microscopy. J. Catal. **255**, 1–5 (2008)
S.B. Simonsen, I. Chorkendorff, S. Dahl, M. Skoglundh, J. Sehested, S. Helveg, Direct observations of oxygen-induced platinum nanoparticle ripening studied by in situ TEM. J. Am. Chem. Soc. **132**, 7968–7975 (2010)
S.B. Simonsen, I. Chorkendorff, S. Dahl, M. Skoglundh, J. Sehested, S. Helveg, Ostwald ripening in a Pt/SiO(2) model catalyst studied by in situ TEM. J. Catal. **281**, 147–155 (2011)
D. Szmigiel, J. Zieliński, H. Bielawa, M. Kurtz, O. Hinrichsen, M. Muhler, W. Rarog, S. Jodzis, Z. Kowalczyk, L. Znak, The kinetics of ammonia synthesis over ruthenium-based catalysts: the role of barium and cesium. J. Catal. **205**, 205–212 (2002)
S.J. Tauster, Strong metal-support interactions. Acc. Chem. Res. **20**, 389–394 (1987)
S.J. Tauster, S.C. Fung, R.L. Garten, Strong metal-support interactions. Group 8 noble metals supported on TiO_2. J. Am. Chem. Soc. **100**, 170–175 (1978)
N.Y. Topsoe, H. Topsoe, FTIR studies of dynamic surface structural changes in Cu-based methanol synthesis catalysts. J. Mol. Catal. A Chem **141**, 95–105 (1999)
N.Y. Topsøe, H. Topsøe, FTIR studies of dynamic surface structural changes in Cu-based methanol synthesis catalysts. J. Mol. Catal. A **141**, 95–105 (1999)
T. Uchiyama, H. Yoshida, Y. Kuwauchi, S. Ichikawa, S. Shimada, M. Haruta, S. Takeda, Systematic morphology changes of gold nanoparticles supported on CeO_2 during CO oxidation. Angew. Chem. Int. Ed. Engl. **50**, 10157–10160 (2011)
B. van Setten, M. Makkee, J.A. Moulijn, Science and technology of catalytic diesel particulate filters. Catal. Rev. Sci. Eng. **43**, 489–564 (2001)
S.B. Vendelbo, C.F. Elkjaer, H. Falsig, I. Puspitasari, P. Dona, L. Mele, B. Morana, B.J. Nelissen, R. van Rijn, J.F. Creemer, P.J. Kooyman, S. Helveg, Visualization of oscillatory behaviour of Pt nanoparticles catalysing CO oxidation. Nat. Mater. (2014)
J.B. Wagner, *In Situ Transmission Electron Microscopy of Catalyst Particles*, in *NBIfAPG*. 2002, University of Copenhagen.
J.B. Wagner, P.L. Hansen, A.M. Molenbroek, H. Topsøe, B.S. Clausen, S. Helveg, In situ electron energy loss spectroscopy studies of gas-dependent metal-support interactions in Cu/ZnO catalysts. J. Phys. Chem. B **107**, 7753–7758 (2003)
D. Waldbillig, A. Wood, D.G. Ivey, Electrochemical and microstructural characterization of the redox tolerance of solid oxide fuel cell anodes. J. Power Sources **145**, 206–215 (2005)
P. Wynblatt, N.A. Gjostein, Supported metal crystallites. Prog. Solid State Chem. **9**, 21–58 (1975)
H. Yoshida, Y. Kuwauchi, J.R. Jinschek, K.J. Sun, S. Tanaka, M. Kohyama, S. Shimada, M. Haruta, S. Takeda, Visualizing gas molecules interacting with supported nanoparticulate catalysts at reaction conditions. Science **335**, 317–319 (2012)
S.R. Zhang, L. Nguyen, Y. Zhu, S.H. Zhan, C.K. Tsung, F. Tao, In-situ studies of nanocatalysis. Acc. Chem. Res. **46**, 1731–1739 (2013a)
L.X. Zhang, B.K. Miller, P.A. Crozier, Atomic level in situ observation of surface amorphization in anatase nanocrystals during light irradiation in water vapor. Nano Lett. **13**, 679–684 (2013b)